

Entanglement detection on an NMR quantum information processor using random local measurements

Amandeep Singh,^{*} Arvind,[†] and Kavita Dorai[‡]

*Department of Physical Sciences, Indian Institute of Science Education & Research (IISER) Mohali,
Sector 81 SAS Nagar, Manauli PO 140306 Punjab India.*

Random local measurements have recently been proposed to construct entanglement witnesses and thereby detect the presence of bipartite entanglement. We experimentally demonstrate the efficacy of one such scheme on a two-qubit NMR quantum information processor. We show that a set of three random local measurements suffices to detect the entanglement of a general two-qubit state. We experimentally generate states with different amounts of entanglement, and show that the scheme is able to clearly witness entanglement. We perform complete quantum state tomography for each state and compute state fidelity to validate our results. Further, we extend previous results and perform a simulation using random local measurements to optimally detect bipartite entanglement in a hybrid system of $2 \otimes 3$ dimensionality.

PACS numbers: 03.67.Bg,03.67.Lx,03.67.Mn

I. INTRODUCTION

Entanglement is an important resource for quantum information processing, and many questions about its characterization, optimal detection and its protection from decoherence are still open [1]. The classification and detection of entanglement is a demanding task and attempts to do so, have relied on methods including those based on Bell-type inequalities [2–4], quantum state tomography [5, 6], dynamic learning tools and numerical schemes [7, 8], entanglement witnesses [9–11], positive partial transpose mixtures [12, 13], and expectation values of Pauli operators [14, 15]. The negativity under partial transpose (NPT) is a necessary and sufficient condition for existence of entanglement in $2 \otimes 2$ and $2 \otimes 3$ dimensional quantum systems [16, 17]. For higher dimensional systems, although a number of sufficient conditions in terms of entanglement witnesses are available, the problem of complete characterization of entanglement is still open [18]. Experimental explorations of entanglement in the context of NMR quantum information processing, include implementation of an entanglement witness [19] and measurement of bipartite quantum correlations of an unknown quantum state [20]. Pseudo-bound entanglement was experimentally generated and ground-state entanglement studied in a system of three NMR qubits [21, 22]. Three-qubit entanglement was characterized on an NMR quantum information processor [23, 24] and the evolution of multiqubit entangled states was studied with a view to control their decoherence [25, 26]. It is important, particularly from an experimental point of view, to be able to detect entanglement by a minimum number of experiments, requiring as little effort as possible.

A promising direction of research in the detection of quantum entanglement has been the use of local observables to find an optimal decomposition of entanglement witnesses [27]. The method assumes some prior knowledge of the density matrix and is able to unequivocally detect entanglement by performing only a few local measurements [28–30]. These entanglement detection schemes have been recently extended to the case of completely unknown states with no prior information [31]. This scheme uses a set of random local measurements and optimizes over the space of possible entanglement witnesses that can be constructed thereof.

This work focuses on experimentally using a set of random local measurements to detect bipartite entanglement of unknown pure entangled states. Our experiments demonstrate the optimality of using random local measurements to detect entanglement in a system of two qubits on an NMR quantum information processor. We obtain the expectation values of a set of local measurement operators and use semi-definite programming to thereby construct the witness operator to detect the presence of entanglement. We show that a set of three local measurements are sufficient to unequivocally detect entanglement of most entangled states of two qubits. We experimentally generate several states with different amounts of entanglement and evaluate their entangled (or separable) nature by performing this optimal set of local measurements. We validate these results by constructing experimental tomographs of each state and compute negativity as a measure of entanglement from them. With a view to generalize these methods to larger spaces, we perform a simulation to detect bipartite entanglement of unknown pure entangled states in a $2 \otimes 3$ system, using a set of random measurements acting locally on the qubit and the qutrit involved. It is observed that by performing a few measurements, the entanglement of most states gets implicated.

The material in the paper is arranged as follows: in Section II we first present the semi-definite programming based protocol to detect entanglement, and later describe

^{*} amandeepsingh@iisermohali.ac.in

[†] arvind@iisermohali.ac.in

[‡] kavita@iisermohali.ac.in

its experimental implementation on two NMR qubits. In Section III we present the results of simulations on a $2 \otimes 3$ system. Section IV contains a few concluding remarks.

II. EXPERIMENTAL DETECTION OF ENTANGLEMENT USING LOCAL MEASUREMENTS

In typical experiments to detect entanglement based on witnesses, knowledge about the state is required beforehand. One may argue that if the state is already known or has been tomographed, then one can calculate its entanglement properties by using the witness. In the present study we take a different approach, where we do not ask for *a priori* state information, but instead strategically choose the local measurements. Semi-definite programming (SDP) is then used to obtain the relative weights of the expectation values of these local measurements which are then used to build the entanglement witness for the unknown state.

We followed the procedure outlined by Szangolies et. al. [31] to construct a class of decomposable entanglement witness operators for an unknown state using random local measurements. In this protocol, once we fix the set of measurements, the witness is optimized to increase the possibility of detecting entanglement. Consider a composite system in a Hilbert space $\mathcal{H}_{AB} = \mathcal{H}_A \otimes \mathcal{H}_B$. A witness operator is a Hermitian operator W in this composite space, such that $\text{Tr}(W\rho) \geq 0$ for all separable ρ and $\text{Tr}(W\rho) \neq 0$ for at least one entangled ρ . A witness is called decomposable if it can be written in terms of two positive operators P and Q such that

$$W = P + Q^{T_A}. \quad (1)$$

where the operation T_A represents the partial transpose with respect to subsystem A . Further, since we would like to build the witness operator out of local measurements, consider local Hermitian operators $A_i \in \mathcal{H}_A$ and $B_j \in \mathcal{H}_B$ where i, j are decided by the number of measurements that we are wish to carry out for each local system. We would therefore like the witness operator to be given as

$$W = \sum_{i,j} c_{ij} A_i \otimes B_j \quad (2)$$

with $c_{ij} \in \mathcal{R}$. It should be noted here that if we allow A_i and B_j to run over a complete set of bases in the local operator spaces, then by Bloch decomposition, every Hermitian operator can be written in the form given in Eqn.(2) as described in [31]. However, in our case we will first choose the measurements that we want to experimentally perform and then optimize the witness operator in such a way that we maximize the chances of detecting entanglement. Finding the expectation value of the entanglement witness operator W (given the set of local observables A_i and B_j) is equivalent to finding

the coefficients c_{ij} subject to the trace constraints on the witness operator. Let us define a column vector \mathbf{c} where we take the columns of c_{ij} and stack them one below the other, and similarly define a vector \mathbf{m} in which we stack the experimentally measured expectation values $\langle A_i \otimes B_j \rangle$ as a long column vector such that

$$\text{Tr}(W\rho) = \sum_{i,j} c_{ij} \langle A_i \otimes B_j \rangle = \mathbf{c} \cdot \mathbf{m} \quad (3)$$

The SDP looks for the class of entanglement witness operators with unit trace and decomposable as $P + Q^{T_A}$. This decomposition ensures the detection of bipartite NPT states. The corresponding SDP can be constructed as [31]:

$$\begin{aligned} &\text{Minimize : } \mathbf{c} \cdot \mathbf{m} \\ &\text{Subject to : (1) } W = \sum_{i,j} c_{ij} (A_i \otimes B_j) \\ &\quad (2) \quad W = P + Q^{T_A} \\ &\quad (3) \quad P \geq 0 \quad \text{and} \quad Q \geq 0 \\ &\quad (4) \quad \text{Tr}(W) = 1 \end{aligned}$$

We implemented the SDP using MATLAB [32] subroutines that employed SeDuMi [33] as an SDP solver.

We now turn to the problem of experimentally measuring the expectation values of various observables using NMR, for a system of N weakly interacting spin-1/2 particles. The density operator for this system can be decomposed as a linear combination of products of Cartesian spin angular momentum operators I_{ni} , n labeling the spin and $i = x, y$ or z [34]. For two qubits a total of 16 product operators completely span the space of all 4×4 Hermitian matrices. The four maximally entangled Bell states for two qubits, and their corresponding entanglement witness operators, can always be written as a linear combination of the three product operators $2I_{1x}I_{2x}$, $2I_{1y}I_{2y}$, $2I_{1z}I_{2z}$ and the identity operator. We use the symbols O_i ($1 \leq i \leq 15$) to represent these product operators, with the first three symbols O_1 , O_2 and O_3 representing the operators $2I_{1x}I_{2x}$, $2I_{1y}I_{2y}$ and $2I_{1z}I_{2z}$ respectively. We need to experimentally determine the expectation values of these operators O_i , for the state ρ whose entanglement is to be characterized. The expectation values of these operators are mapped to the local z -magnetization of either of the two qubits by specially crafted NMR pulse sequences, and are summarized in Table I. The expectation values are obtained by measuring the z -magnetizations of the corresponding qubit. The NMR pulse sequences given in Table I transform the state via a single measurement, which is completely equivalent to the originally intended measurement of local operators, and considerably simplifies the experimental protocol.

The two NMR qubits were encoded in a molecule of ^{13}C enriched chloroform, with the ^1H and ^{13}C nuclei being labeled as the first and the second qubit, respectively. The molecular structure, experimental parameters, and

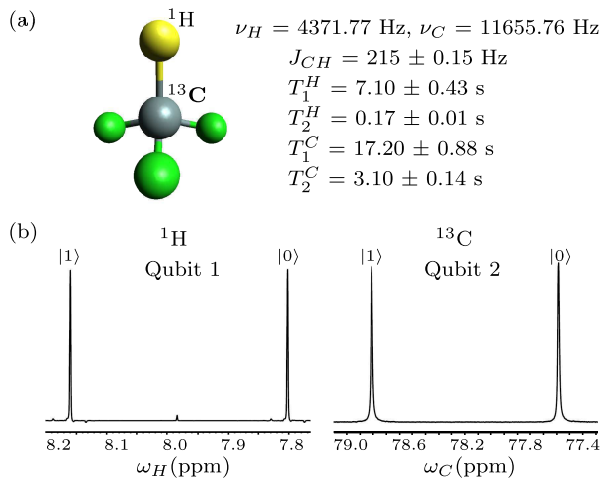


FIG. 1. (Color online) (a) Structure of the ^{13}C enriched chloroform molecule with the two qubits labeled as ^1H and ^{13}C . Tabulated experimental NMR parameters with chemical shifts (ν_i) and spin-spin coupling (J_{ij}) in Hz, and relaxation times T_1 and T_2 in seconds, and (b) ^1H and ^{13}C NMR spectra obtained at thermal equilibrium after a $\frac{\pi}{2}$ readout pulse. The spectral resonances of each qubit are labeled by the logical state $\{|0\rangle, |1\rangle\}$ of the other qubit.

the NMR spectrum of the thermal initial state are shown in Fig.1. Experiments were performed at room temperature on a Bruker Avance III 600 MHz NMR spectrometer equipped with a QXI probe. The Hamiltonian of this weakly interacting two-qubit system in the rotating frame [34] is

$$\mathcal{H} = \nu_H I_z^H + \nu_C I_z^C + J_{CH} I_z^H I_z^C \quad (4)$$

where ν_H, ν_C are the Larmor resonance frequencies and I_z^H, I_z^C are the z components of the spin angular momentum operators for the proton and carbon nuclei respectively, and J_{CH} is the spin-spin coupling constant.

The two-qubit system was initially prepared in the pseudopure state $|00\rangle$ using the spatial averaging technique [35], with the density operator given by

$$\rho_{00} = \frac{1}{4}(1 - \epsilon)I + \epsilon|00\rangle\langle 00| \quad (5)$$

where $\epsilon \approx 10^{-5}$ is an estimate of the thermal polarization. We note here that NMR is an ensemble technique that can experimentally observe only deviation density matrices (with zero trace). The state fidelity was calculated from the Uhlmann-Jozsa relation [36, 37]

$$F = \left(\text{Tr} \left(\sqrt{\sqrt{\rho_{th}} \rho_{ex} \sqrt{\rho_{th}}} \right) \right)^2 \quad (6)$$

where ρ_{th} and ρ_{ex} represent the theoretical and experimentally prepared density matrices respectively. The experimentally prepared pseudopure state was tomographed using full quantum state tomography [38] and the state fidelity was computed to be 0.99 ± 0.01 .

TABLE I. All fifteen observables for two qubits, mapped to the local z -magnetization of one of the qubits. This mapping allows a simpler method to measure the expectation values of the operators O_j and is completely equivalent to the measurement of the original local operators.

Observable	Initial State Mapped to
$\langle O_1 \rangle = \text{Tr}[\rho_1 \cdot I_{2z}]$	$\rho_1 = \text{CNOT} \cdot Y_2 \cdot Y_1 \cdot \rho_0 \cdot Y_1^\dagger \cdot Y_2^\dagger \cdot \text{CNOT}^\dagger$
$\langle O_2 \rangle = \text{Tr}[\rho_2 \cdot I_{2z}]$	$\rho_2 = \text{CNOT} \cdot \bar{X}_2 \cdot \bar{X}_1 \cdot \rho_0 \cdot \bar{X}_1^\dagger \cdot \bar{X}_2^\dagger \cdot \text{CNOT}^\dagger$
$\langle O_3 \rangle = \text{Tr}[\rho_3 \cdot I_{2z}]$	$\rho_3 = \text{CNOT} \cdot \rho_0 \cdot \text{CNOT}^\dagger$
$\langle O_4 \rangle = \text{Tr}[\rho_4 \cdot I_{2z}]$	$\rho_4 = \text{CNOT} \cdot \bar{X}_2 \cdot Y_1 \cdot \rho_0 \cdot Y_1^\dagger \cdot \bar{X}_2^\dagger \cdot \text{CNOT}^\dagger$
$\langle O_5 \rangle = \text{Tr}[\rho_5 \cdot I_{2z}]$	$\rho_5 = \text{CNOT} \cdot Y_1 \cdot \rho_0 \cdot Y_1^\dagger \cdot \text{CNOT}^\dagger$
$\langle O_6 \rangle = \text{Tr}[\rho_6 \cdot I_{2z}]$	$\rho_6 = \text{CNOT} \cdot \bar{Y}_2 \cdot X_1 \cdot \rho_0 \cdot X_1^\dagger \cdot \bar{Y}_2^\dagger \cdot \text{CNOT}^\dagger$
$\langle O_7 \rangle = \text{Tr}[\rho_7 \cdot I_{2z}]$	$\rho_7 = \text{CNOT} \cdot X_1 \cdot \rho_0 \cdot X_1^\dagger \cdot \text{CNOT}^\dagger$
$\langle O_8 \rangle = \text{Tr}[\rho_8 \cdot I_{2z}]$	$\rho_8 = \text{CNOT} \cdot \bar{Y}_2 \cdot \rho_0 \cdot \bar{Y}_2^\dagger \cdot \text{CNOT}^\dagger$
$\langle O_9 \rangle = \text{Tr}[\rho_9 \cdot I_{2z}]$	$\rho_9 = \text{CNOT} \cdot X_2 \cdot \rho_0 \cdot X_2^\dagger \cdot \text{CNOT}^\dagger$
$\langle O_{10} \rangle = \text{Tr}[\rho_{10} \cdot I_{1z}]$	$\rho_{10} = \bar{Y}_1 \cdot \rho_0 \cdot \bar{Y}_1^\dagger$
$\langle O_{11} \rangle = \text{Tr}[\rho_{11} \cdot I_{1z}]$	$\rho_{11} = X_1 \cdot \rho_0 \cdot X_1^\dagger$
$\langle O_{12} \rangle = \text{Tr}[\rho_{12} \cdot I_{1z}]$	ρ_{12} is initial state
$\langle O_{13} \rangle = \text{Tr}[\rho_{13} \cdot I_{2z}]$	$\rho_{13} = \bar{Y}_2 \cdot \rho_0 \cdot \bar{Y}_2^\dagger$
$\langle O_{14} \rangle = \text{Tr}[\rho_{14} \cdot I_{2z}]$	$\rho_{14} = X_2 \cdot \rho_0 \cdot X_2^\dagger$
$\langle O_{15} \rangle = \text{Tr}[\rho_{15} \cdot I_{2z}]$	ρ_{15} is initial state

The quantum circuit to implement the two-qubit entanglement detection protocol is shown in Fig.2(a). The first block in the circuit (enclosed in a dashed red box) transforms the $|00\rangle$ pseudopure state to an entangled state with a desired amount of entanglement. Control of the entanglement present in the state was achieved by controlling the time evolution under the non-local interaction Hamiltonian. A CNOT gate that achieves this control is represented by a dashed line. The next block of the circuit (enclosed in a dashed red box), maps any one of the observables $\langle O_i \rangle$ ($1 \leq i \leq 15$) to the local z -magnetization of one of the qubits, with U_1^i and U_2^j representing local unitaries (as represented in Table I). The dashed green box represents the measurement. Only one measurement is performed in a single experiment.

The NMR pulse sequence to implement the quantum circuit for entanglement detection using random local measurements, starting from the pseudopure state $|00\rangle$ is shown in Fig.2(b). Unfilled rectangles represent $\frac{\pi}{2}$ pulses while solid rectangles denote π pulses. Refocusing pulses were used in the middle of all J -evolution periods to compensate for undesired chemical shift evolution. Composite pulses are represented by z in the pulse sequence, where each composite- z rotation is a sandwich of three pulses: $xy\bar{x}$. The CNOT gate represented by the dashed line in Fig.2(a), was achieved experimentally by controlling the evolution time τ_i , and the angle of z -rotation (the grey-shaded rectangle); ϕ_1^i and ϕ_2^j are local rotations, and depend upon which $\langle O_i \rangle$ value is being measured, and the τ time interval was set to $\tau = \frac{1}{2J_{CH}}$.

We begin by describing an explicit example to demonstrate how the SDP can be used to construct an en-

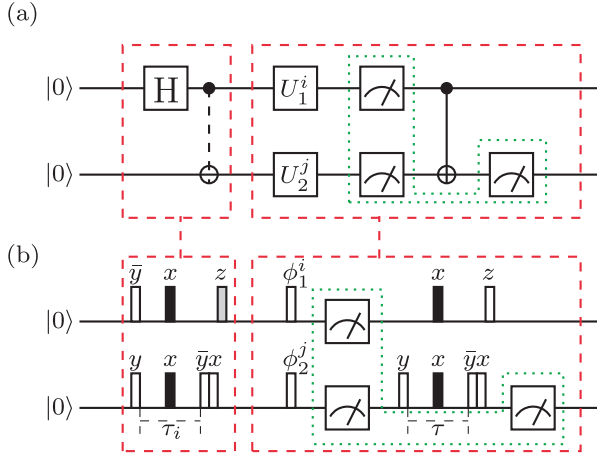


FIG. 2. (Color online) (a) Quantum circuit to implement the entanglement detection protocol. The first red box creates entangled states with different amounts of entanglement. The second red box maps the observables O_i to the z -magnetization of either qubit. Only one z -magnetization is finally measured in an experiment (inner green box). (b) NMR pulse sequence for the quantum circuit. Unfilled rectangles represent $\frac{\pi}{2}$ pulses, while solid rectangles represent π pulses. Tuning of the interaction between qubits is controlled by varying the τ_i time period and the z -pulse rotation angle (grey rectangular shape). Pulse phases are written above each pulse, with a bar indicating negative phase. The τ evolution period was fixed at $\frac{1}{4J_{CH}}$, where J_{CH} is the strength of the scalar coupling.

tanglement witness. Consider the Bell state $|\phi^-\rangle = \frac{1}{\sqrt{2}}(|00\rangle - |11\rangle)$. The corresponding density matrix can be written as a linear superposition of product operators:

$$\rho = \frac{I}{4} + a2I_{1x}I_{2x} + b2I_{1y}I_{2y} + c2I_{1z}I_{2z} \quad (7)$$

where $b = c = -a = \frac{1}{2}$. Since it is known that the given state is entangled, the corresponding entanglement witness can be constructed as [18]:

$$W_{\phi^-} = c_{opt}I - \rho = \frac{I}{4} - a2I_{1x}I_{2x} - b2I_{1y}I_{2y} - c2I_{1z}I_{2z} \quad (8)$$

where c_{opt} is the smallest possible value such that the witness is positive on all separable states; for Bell states c_{opt} is $\frac{1}{2}$. Noting that $\text{Tr}(\rho W_{\phi^-}) = -\frac{1}{2} < 0$, hence by definition W_{ϕ^-} detects the presence of entanglement in ρ . However, our detection protocol has to deal with the situation when the state is unknown. The question now arises whether the SDP method is able to find the minimum value of $\mathbf{c} \cdot \mathbf{m}$ such that the correct W_{ϕ^-} is constructed? For the Bell state $|\phi^-\rangle$, the expectation values for $\langle O_1 \rangle$, $\langle O_2 \rangle$ and $\langle O_3 \rangle$ yield $-\frac{1}{2}$, $\frac{1}{2}$ and $\frac{1}{2}$ respectively. The experimental NMR spectra obtained after measuring $\langle O_1 \rangle$, $\langle O_2 \rangle$ and $\langle O_3 \rangle$ are shown in Fig.3, with measured expectation values of -0.490 ± 0.021 , 0.487 ± 0.030 and 0.479 ± 0.015 respectively (these values correspond to the area under the absorptive peaks normalized with

respect to the pseudopure state). These experimental expectation values are used to construct the vector \mathbf{m} . The SDP protocol performs minimization under the given constraints and for this Bell state, is indeed able to construct W_{ϕ^-} as well as the exact values of a , b and c which make up the vector \mathbf{c} . Since the minimum value of $\mathbf{c} \cdot \mathbf{m} < 0$ is achieved, it confirms the presence of entanglement in the state.

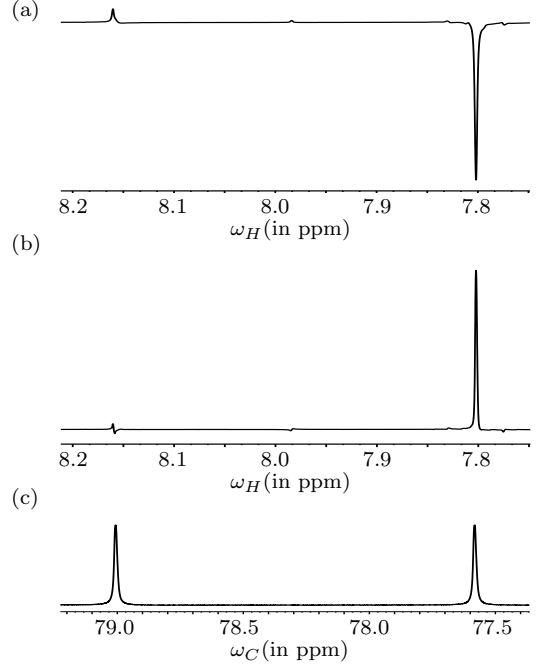


FIG. 3. NMR spectra of ^1H and ^{13}C nuclei, showing the experimentally measured expectation values of (a) $\langle O_1 \rangle$, (b) $\langle O_2 \rangle$, and (c) $\langle O_3 \rangle$ respectively, of the Bell state $|\phi^-\rangle = \frac{1}{\sqrt{2}}(|00\rangle - |11\rangle)$. The expectation values have been measured by the NMR pulse sequences given in Table I.

We now turn to the detection of entanglement in states with varying amounts of entanglement. We experimentally implemented the entanglement detection protocol on several different states: four maximally entangled states (labeled as B_1 , B_2 etc), two separable states (labeled as S_1 and S_2) and fourteen non-maximally entangled states (labeled as E_1 , E_2 , E_3 ...). To prepare the fourteen entangled states E_1 to E_{14} (having different amounts of entanglement), the control on the amount of entanglement in the state was achieved by varying the time interval τ_i and the angle (θ) of the z -rotation (Fig.2(b)). We used $\theta = n\frac{\pi}{30}$ and $\tau_i = n\frac{1}{30J}$ with $1 \leq n \leq 14$. These choices for θ and τ_i represent a variation of the rotation angle in a two-qubit controlled-rotation NMR gate and led to a wide range of entanglement in the generated states (as tabulated in Table II). To characterize the amount of entanglement, we used the negativity \mathcal{N} [16] as entanglement parameter:

$$\mathcal{N} = \|\rho^{PT}\| - 1 \quad (9)$$

where ρ^{PT} denotes partial transpose with respect to one

TABLE II. Results of entanglement detection via local measurements followed by SDP. States are labeled as B , S or E indicating maximally entangled, separable or non-maximally entangled respectively. The second and third columns contain the theoretically expected and experimentally obtained values of the entanglement negativity (\mathcal{N}). The \checkmark in the last column indicates the success of the experimental protocol in detecting entanglement.

State	\mathcal{N}		Entanglement Detected
	Theory	Exp	
B_1	0.500	0.486 ± 0.011	\checkmark
B_2	0.500	0.480 ± 0.013	\checkmark
B_3	0.500	0.471 ± 0.021	\checkmark
B_4	0.500	0.466 ± 0.025	\checkmark
S_1	0.000	0.000 ± 0.000	\checkmark
S_2	0.000	0.000 ± 0.000	\checkmark
E_1	0.052	0.081 ± 0.005	\times
E_2	0.104	0.088 ± 0.024	\times
E_3	0.155	0.177 ± 0.015	\checkmark
E_4	0.203	0.182 ± 0.031	\checkmark
E_5	0.250	0.212 ± 0.029	\checkmark
E_6	0.294	0.255 ± 0.033	\checkmark
E_7	0.335	0.297 ± 0.045	\checkmark
E_8	0.372	0.351 ± 0.039	\checkmark
E_9	0.405	0.400 ± 0.033	\checkmark
E_{10}	0.433	0.410 ± 0.040	\checkmark
E_{11}	0.457	0.430 ± 0.037	\checkmark
E_{12}	0.476	0.444 ± 0.029	\checkmark
E_{13}	0.489	0.462 ± 0.022	\checkmark
E_{14}	0.497	0.473 ± 0.025	\checkmark

of the qubits, and $\|\cdot\|$ represent the trace norm. A non-zero negativity confirms the presence of entanglement in ρ and can be used as a quantitative measure of entanglement. The states prepared ranged from nearly separable (E_1, E_2 with a low value of negativity) to nearly maximally entangled (E_{13}, E_{14} with high negativity values). The experimental results of the entanglement detection protocol for two qubits are tabulated in Table II. For some of the non-maximally entangled states, more than three local measurements had to be used to detect entanglement. For instance, SDP required six local measurement to build the vector \mathbf{m} for the E_8 state in Table II, and to establish that $\text{Minimum}(\mathbf{c} \cdot \mathbf{m}) < 0$. As is evident from Table II, this method of making random local measurements on an unknown state followed by SDP to construct an entanglement witness, is able to successfully detect the presence of quantum entanglement in almost all the experimentally created states. The protocol failed to detect entanglement in the states E_1 and E_2 , a possible reason for this being that these states have a very low negativity value (very little entanglement), which is of the order of the experimental error. In order to validate our experimental results we also performed quantum

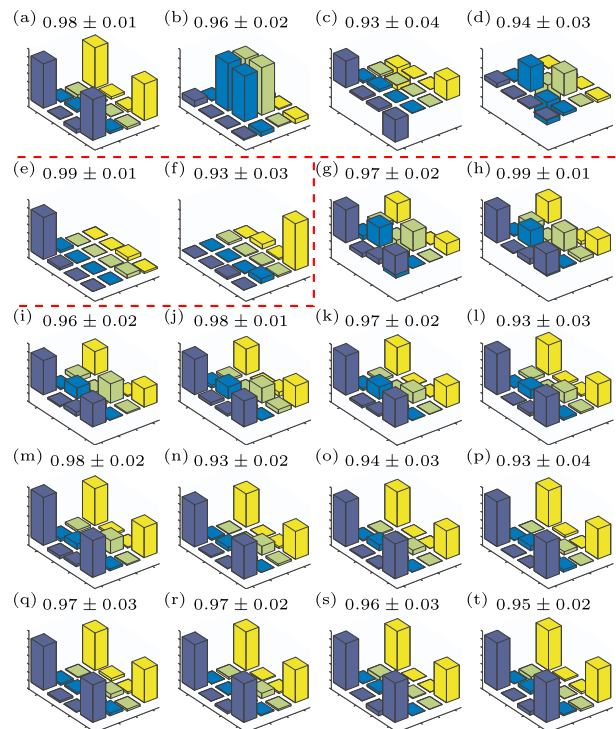


FIG. 4. (Color online) Real part of the tomographed density matrix for the states described in Table II. Maximally entangled Bell states are shown in (a)-(d), while separable states are shown in (e)-(f). The tomographs (g)-(t) represent states of different degrees of entanglement. The state fidelity is written above each tomograph. The arrangement of the rows and columns of the bar graphs is as per the computational basis of the two-qubit system $\{|00\rangle, |01\rangle, |10\rangle, |11\rangle\}$.

state tomography of all experimentally prepared states. The resulting tomographs and respective fidelities are shown in Fig.4 and the negativity parameter obtained from the experimental tomographs in each case is tabulated in Table II. Fig.4(a)-(d) correspond to the maximally entangled Bell states B_1 to B_4 respectively, while Fig.4(e) and (f) are tomographs for the separable states S_1 and S_2 respectively, and Fig.4(g)-(t) correspond to the states E_1 to E_{14} respectively. The fidelity of each experimentally prepared state is given above its tomograph in the figure. Only the real parts of the experimental tomographs are shown, as the imaginary parts of the experimental tomographs turned out to be negligible.

III. DETECTING ENTANGLEMENT IN BIPARTITE $2 \otimes 3$ DIMENSIONAL SYSTEMS

The orthonormal basis states for a $2 \otimes 3$ -dimensional qubit-qutrit system $\{|ij\rangle : i = 0, 1, j = 0, 1, 2\}$ can be written in the computational basis for the qubit ($\{|0\rangle, |1\rangle\}$) and the qutrit ($\{|0\rangle, |1\rangle, |2\rangle\}$) respectively. It has been previously shown that any arbitrary pure state of a hybrid qubit-qutrit $2 \otimes 3$ system can be transformed

to one of the states of a two-parameter class (with two real parameters), via local operations and classical communication (LOCC), and that states in this class are invariant under unitary operations of the form $U \otimes U$ on the $2 \otimes 3$ system [39]. The state for such a bipartite $2 \otimes 3$ dimensional system can be written as [39]

$$\rho = \alpha [|02\rangle\langle 02| + |12\rangle\langle 12|] + \beta [| \phi^+ \rangle\langle \phi^+ | + | \phi^- \rangle\langle \phi^- | + | \psi^+ \rangle\langle \psi^+ | + \gamma | \psi^- \rangle\langle \psi^- | \quad (10)$$

where

$$| \phi^\pm \rangle = \frac{1}{\sqrt{2}} (|00\rangle \pm |11\rangle) \text{ and } | \psi^\pm \rangle = \frac{1}{\sqrt{2}} (|01\rangle \pm |10\rangle) \quad (11)$$

are the maximally entangled Bell states.

The requirement of unit trace places a constraint on the real parameters α, β and γ

$$2\alpha + 3\beta + \gamma = 1 \quad (12)$$

This constraint implies that one can eliminate one of the three parameters and we have chosen to rewrite β in terms of α and γ ; however the entire analysis is valid for the other choices as well. The domains for α, γ can be calculated from the unit trace condition and turn out to be $0 \leq \alpha \leq 1/2$ and $0 \leq \gamma \leq 1$.

The Peres-Horodecki positive partial transposition (PPT) criterion is a necessary and sufficient condition for $2 \otimes 3$ dimensional systems, and can hence be used to characterize the entanglement of ρ via the entanglement parameter termed negativity (\mathcal{N}). The partial transpose with respect to the qubit, for the two-parameter class of states defined in Eqn.(10) can be written as

$$\rho^{PT} = \alpha [|02\rangle\langle 02| + |12\rangle\langle 12|] + \frac{(\beta + \gamma)}{2} [|01\rangle\langle 01| + |10\rangle\langle 10| + | \phi^- \rangle\langle \phi^- |] + \frac{(3\beta - \gamma)}{2} | \phi^+ \rangle\langle \phi^+ | \quad (13)$$

The negativity $\mathcal{N}(\rho)$ for the two-parameter class of states can be calculated from its partial transpose and is given by [39]:

$$\mathcal{N}(\rho) = \max\{(2\alpha + 2\gamma - 1), 0\} \quad (14)$$

Clearly, states with $1/2 < \alpha + \gamma \leq 1$ have non-zero negativity (i.e. are NPT) and are hence entangled.

We extend the Bloch representation for qubits to a qubit-qutrit system described by a $2 \otimes 3$ dimensional hybrid linear vector space. An operator O operating on this combined space can be written as [40]

$$O = \frac{1}{6} [I_2 \otimes I_3 + \sigma^A \cdot \vec{u} \otimes I_3 + \sqrt{3} I_2 \otimes \lambda^B \cdot \vec{v} + \sum_{i=1}^3 \sum_{j=1}^8 \beta_{ij} (\sigma^A_i \otimes \lambda^B_j)] \quad (15)$$

where \vec{u} and \vec{v} are vectors belonging to a linear vector space of dimension 3 and 8 respectively, I_2 and I_3

are identity matrices of dimensions 2 and 3, σ_i are the Pauli spin matrices used to span operators acting on the Hilbert space of the qubit, and λ_j are the Gell-Mann matrices [41], used to span operators acting on the Hilbert space of the qutrit; other isomorphic choices are equally valid.

A Hermitian witness operator can be constructed for every entangled quantum state and the expectation value of the witness operator can be locally measured by decomposing the operator as a weighted sum of projectors onto product state vectors [16, 42, 43]. The ρ for the $2 \otimes 3$ system given in Eqn.(10) is NPT for $0.5 < (\alpha + \gamma) \leq 1$. The eigenvalues for ρ^{PT} (where PT represents partial transposition with respect to the qubit) are: α , $\frac{1}{2}(1 - 2\alpha - 2\gamma)$ and $\frac{1}{6}(1 - 2\alpha + 2\gamma)$. The eigenvalue $\frac{1}{2}(1 - 2\alpha - 2\gamma)$ remains negative for NPT states and we denote its corresponding eigenvector by $|\eta\rangle$. The corresponding entanglement witness operator can be written as $W = (|\eta\rangle\langle\eta|)^{PT}$ with its matrix representation

$$W = \begin{pmatrix} \frac{1}{2} & 0 & 0 & 0 & 0 & 0 \\ 0 & 0 & 0 & \frac{1}{2} & 0 & 0 \\ 0 & 0 & 0 & 0 & 0 & 0 \\ 0 & \frac{1}{2} & 0 & 0 & 0 & 0 \\ 0 & 0 & 0 & 0 & 0 & 0 \\ 0 & 0 & 0 & 0 & 0 & \frac{1}{2} \end{pmatrix} \quad (16)$$

The entanglement witness W is capable of detecting entanglement of the $2 \otimes 3$ dimensional ρ given in Eqn.(10).

We now turn to the decomposition of the entanglement witness W in terms of local observables, so that we can use it to detect entanglement of the two-parameter class of states of the $2 \otimes 3$ dimensional ρ . The explicit decomposition of W as per Eqn.(15) results in the following:

$$\vec{u} = \begin{bmatrix} 0 \\ 0 \\ 0 \\ 0 \\ 0 \\ 0 \\ 0 \\ 1 \end{bmatrix}, \quad \vec{v} = \begin{bmatrix} 0 \\ 0 \\ 0 \\ 0 \\ 0 \\ 0 \\ 0 \\ 1 \end{bmatrix}, \quad \beta = \begin{bmatrix} \frac{1}{2} & 0 & 0 & 0 & 0 & 0 & 0 & 0 \\ 0 & \frac{1}{2} & 0 & 0 & 0 & 0 & 0 & 0 \\ 0 & 0 & \frac{1}{2} & 0 & 0 & 0 & 0 & 0 \end{bmatrix} \quad (17)$$

The components of \vec{u} and \vec{v} i.e. u_i ($i = 1, 2, 3$) and v_j ($j = 1, 2, 3, \dots, 8$) were obtained from $u_i = \text{Tr}[W(\sigma_i \otimes I_3)]$ and $v_j = \text{Tr}[W(I_2 \otimes \lambda_j)]$. Similarly the elements of the matrix β can be obtained from $\beta_{ij} = \text{Tr}[W(\sigma_i \otimes \lambda_j)]$. There are thirty five real coefficients in the expansion in Eqn.(15), of which three coefficients constitute \vec{u} , eight coefficients constitute \vec{v} and the remaining twenty four are contained in the β matrix. Each non-zero entry in \vec{u} , \vec{v} or the β matrix is the contribution of the corresponding qubit-qutrit product operator [34] used in the construction of operator W . Hence one can infer by inspection of the non-zero matrix entries in Eqn.(17), that one requires the

expectation values of at least four operators in a given state, in order to experimentally construct the witness operator W .

While the maximum number of expectation values required to be measured is four, the question remains if this is an optimal set or can we find a smaller set which will still be able to detect entanglement. We hence computed the fraction of entanglement detected, by gradually increasing the number of local observations, and the results of the simulation are depicted in Fig.5(a) as a bar chart. We note here that even if we measure only one observable (one element of the β matrix in Eqn.(17)), half of the randomly generated entangled states are detected. As the number of measured observables is increased, the fraction of detected entangled states improves, as shown in Fig.5(a). To generate the bar plots in Fig.5, we began by selecting only one random local measurement out of the maximum thirty five possible measurements. Only those choices are valid which will establish a decomposable entanglement witness of unit trace. For one such choice (denoted by W_I), the $\text{Tr}(W_I\rho)$ is plotted in Fig.5(b) in the range $0 \leq \alpha \leq 0.5$ and $0 \leq \gamma \leq 1$. As is evident, this W_I (based on only one random local measurement) does not detect all the entangled states which were detected by W . The fraction of entangled states detected by W_I can be computed from geometry i.e. how much area that is spanned by the parameters α and γ represents entangled states and how much of that area is detected by the corresponding entanglement witness operator. When we consider random local measurements chosen two at a time, to construct a valid entanglement witness (W_{II} in Fig.5(c)), the detected fraction of entangled states improves from 0.50 to 0.67 (the second bar in Fig.5(a)). One can observe from the geometry that W_{II} detects more entangled states as compared to W_I , but this fraction is still smaller than those detected by W . The result of choosing three random local measurements (denoted by witness operator W_{III}) is plotted in Fig.5(d), and this detects 83.3% of the total entangled states (the third bar in Fig.5(a)). Increasing the set of random local measurements hence increases the probability of detecting entanglement. The worst case detection fraction is shown in Fig.5(a), when choosing random local measurements. A fraction of 1 in the Fig.5(a) implies that the corresponding set of four random local measurements, will always be able to detect entanglement in the state, if it exists.

IV. CONCLUDING REMARKS

We have experimentally demonstrated how a scheme based on local random measurements detects the presence of entanglement, on a two-qubit NMR quantum information processor. An optimal set of random local

measurements was arrived at via semi-definite programming to construct entanglement witnesses that detect bipartite entanglement. The local measurements on each

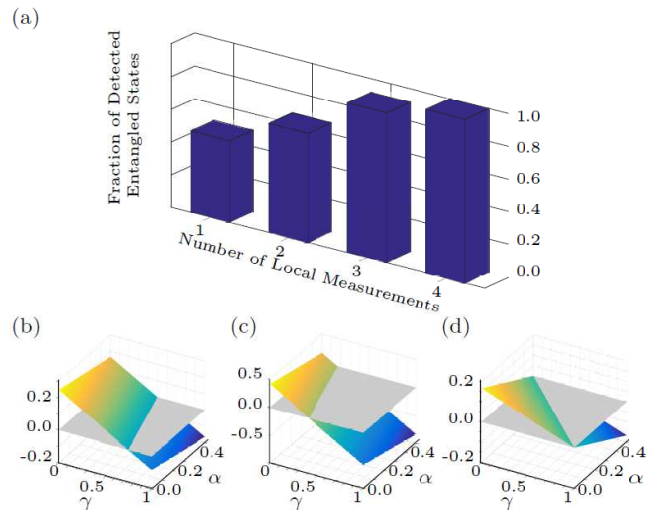


FIG. 5. (Color online) (a) Bar graph showing the fraction of the detected entangled states plotted as a function of the number of local measurements, from the simulation on the qubit-qutrit system. Panels (b), (c), (d) show plots of $\text{Tr}(W_I\rho_{AB})$, $\text{Tr}(W_{II}\rho_{AB})$, and $\text{Tr}(W_{III}\rho_{AB})$ respectively, for $0 \leq \alpha \leq 0.5$ and $0 \leq \gamma \leq 1$. The entanglement witness operators W_I, W_{II}, W_{III} are constructed by choosing sets of one, two or three random local measurements at a time, respectively. A reference plane (gray-shaded) at vanishing trace is also plotted to better differentiate positive and negative values.

qubit were converted into a single measurement on one of the qubits by transforming the state. This was done to simplify the experimental scheme and is completely equivalent to the originally intended local measurements.

We have extended the scheme based on random local measurements to hybrid systems, where qudits of different dimensionality are involved. For the particular case of a qubit-qutrit system, we perform a simulation to demonstrate the optimality of the detection scheme. Characterization of entangled states of qudits is a daunting task, and this work holds promise for further research in this direction. Efforts are on to extend the scheme to experimentally detect the presence of multipartite entanglement in systems of three and more coupled qubits.

ACKNOWLEDGMENTS

All experiments were performed on a Bruker Avance-III 600 MHz FT-NMR spectrometer at the NMR Research Facility at IISER Mohali. Arvind acknowledges funding from DST India under Grant number EMR/2014/000297. KD acknowledges funding from DST India under Grant number EMR/2015/000556.

-
- [1] R. Horodecki, P. Horodecki, M. Horodecki, and K. Horodecki, *Rev. Mod. Phys.*, **81**, 865 (2009).
- [2] M. Huber, H. Schimpf, A. Gabriel, C. Spengler, D. Bruss, and B. C. Hiesmayr, *Phys. Rev. A*, **83**, 022328 (2011).
- [3] B. Jungnitsch, T. Moroder, and O. Guhne, *Phys. Rev. Lett.*, **106**, 190502 (2011).
- [4] J. J. Wallman and S. D. Bartlett, *Phys. Rev. A*, **85**, 024101 (2012).
- [5] A. G. White, D. F. V. James, P. H. Eberhard, and P. G. Kwiat, *Phys. Rev. Lett.*, **83**, 3103 (1999).
- [6] R. T. Thew, K. Nemoto, A. G. White, and W. J. Munro, *Phys. Rev. A*, **66**, 012303 (2002).
- [7] E. C. Behrman and J. E. Steck, *Quant. Inf. Comp.*, **13**, 36 (2013).
- [8] F. M. Spedalieri, *Phys. Rev. A*, **86**, 062311 (2012).
- [9] M. Lewenstein, B. Kraus, J. I. Cirac, and P. Horodecki, *Phys. Rev. A*, **62**, 052310 (2000).
- [10] O. Guhne, P. Hyllus, D. Bruss, A. Ekert, M. Lewenstein, C. Macchiavello, and A. Sanpera, *J. Mod. Opt.*, **50**, 1079 (2003).
- [11] J. M. Arrazola, O. Gittsovich, and N. Lutkenhaus, *Phys. Rev. A*, **85**, 062327 (2012).
- [12] L. Novo, T. Moroder, and O. Guhne, *Phys. Rev. A*, **88**, 012305 (2013).
- [13] K. Bartkiewicz, J. Beran, K. Lemr, M. Norek, and A. Miranowicz, *Phys. Rev. A*, **91**, 022323 (2015).
- [14] M.-J. Zhao, T.-G. Zhang, X. Li-Jost, and S.-M. Fei, *Phys. Rev. A*, **87**, 012316 (2013).
- [15] A. Miranowicz, K. Bartkiewicz, J. P. Jr, M. Koashi, N. Imoto, and F. Nori, *Phys. Rev. A*, **90**, 062123 (2014).
- [16] M. Horodecki, P. Horodecki, and R. Horodecki, *Phys. Lett. A*, **223**, 1 (1996).
- [17] A. Peres, *Phys. Rev. Lett.*, **77**, 1413 (1996).
- [18] O. Guhne and G. Toth, *Phys. Rep.*, **474**, 1 (2009).
- [19] J. G. Filgueiras, T. O. Maciel, R. E. Auccaise, R. O. Vianna, R. S. Sarthour, and I. S. Oliveira, *Quant. Inf. Process.*, **11**, 1883 (2012).
- [20] I. A. Silva, D. Girolami, R. Auccaise, R. S. Sarthour, I. S. Oliveira, T. J. Bonagamba, E. R. deAzevedo, D. O. Soares-Pinto, and G. Adesso, *Phys. Rev. Lett.*, **110**, 140501 (2013).
- [21] H. Kampermann, D. Bruss, X. Peng, and D. Suter, *Phys. Rev. A*, **81**, 040304 (2010).
- [22] X. Peng, J. Zhang, J. Du, and D. Suter, *Phys. Rev. A*, **81**, 042327 (2010).
- [23] S. Dogra, K. Dorai, and Arvind, *Phys. Rev. A*, **91**, 022312 (2015).
- [24] D. Das, S. Dogra, K. Dorai, and Arvind, *Phys. Rev. A*, **92**, 022307 (2015).
- [25] M. Kawamura, T. Morimoto, Y. Mori, R. Sawae, K. Takarabe, and Y. Manmoto, *Int. J. Qtm. Chem.*, **106**, 3108 (2006).
- [26] H. Singh, Arvind, and K. Dorai, *Phys. Rev. A*, **90**, 052329 (2014).
- [27] O. Guhne, P. Hyllus, D. Bruss, A. Ekert, M. Lewenstein, C. Macchiavello, and A. Sanpera, *Phys. Rev. A*, **66**, 062305 (2002).
- [28] O. Guhne and P. Hyllus, *Int. J. Theor. Phys.*, **42**, 1001 (2003).
- [29] G. Toth and O. Guhne, *Phys. Rev. Lett.*, **94**, 060501 (2005).
- [30] O. Guhne and M. Seevinck, *New J. Phys.*, **12**, 053002 (2010).
- [31] J. Szangolies, H. Kampermann, and D. Bruss, *New J. Phys.*, **17**, 113051 (2015).
- [32] MATLAB, *Version 8.5.0 (R2015a)* (MathWorks Inc., Natick, Massachusetts, 2015).
- [33] J. F. Sturm, *Opt. Meth. Soft.*, **11**, 625 (1999).
- [34] R. R. Ernst, G. Bodenhausen, and A. Wokaun, *Principles of Nuclear Magnetic Resonance in One and Two Dimensions (International Series of Monographs on Chemistry)* (Clarendon Press, Oxford, United Kingdom, 1990).
- [35] D. Cory, M. Price, and T. Havel, *Physica D*, **120**, 82 (1998).
- [36] A. Uhlmann, *Rep. Math. Phys.*, **9**, 273 (1976).
- [37] R. Jozsa, *J. Mod. Opt.*, **41**, 2315 (1994).
- [38] G. M. Leskowitz and L. J. Mueller, *Phys. Rev. A*, **69**, 052302 (2004).
- [39] D. P. Chi and S. Lee, *J. Phys. A: Math. Gen.*, **36**, 11503 (2003).
- [40] S. Jami and M. Sarbishei, *Indian J. Phys.*, **79**, 167 (2005).
- [41] M. Gell-Mann and Y. Neeman, *The Eightfold Way* (W. A. Benjamin Inc., New York, 1964).
- [42] M. Bourennane, M. Eibl, C. Kurtsiefer, S. Gaertner, H. Weinfurter, O. Guhne, P. Hyllus, D. Bruss, M. Lewenstein, and A. Sanpera, *Phys. Rev. Lett.*, **92**, 087902 (2004).
- [43] F. G. S. L. Brandao, *Phys. Rev. A*, **72**, 022310 (2005).